Review Article | Cardiovascular Imaging

eISSN 2005-8330
https://doi.org/10.3348/kjr.2024.0261
Korean J Radiol 2026;27(3):227-243

Korean Journal of Radiology
KJR

Photon-Counting CT in Cardiovascular Imaging: Clinical Applications

Prabhakar Shantha Rajiah[1], James M. Williams[1,2], Michael LaVere[1], Shuai Leng[1], Phillip M. Young[1]

[1]Department of Radiology, Mayo Clinic, Rochester, MN, USA
[2]Department of Radiology, Kingman Regional Medical Center, Kingman, AZ, USA

Photon-counting CT (PCCT) uses semiconductor detectors to directly convert X-ray photons to electrical signals, the intensity of which is directly proportional to the energy of the individual photons. PCCT offers several advantages in cardiovascular imaging, including ultra-high-resolution (UHR) imaging, improved multi-energy capabilities, reduced noise and artifacts, and improved iodine signal and radiation dose efficiencies. UHR imaging enhances the assessment of small vessels, dense calcifications, and stents. Multienergy mode enhances the iodine signal, reduces artifacts, and allows for material separation and lesion characterization. In this article, we review PCCT technology, highlight the benefits of PCCT in cardiovascular imaging using case examples, and discuss its challenges.

Keywords: CT; Photon-counting CT; Cardiac imaging; Stent; Plaque

INTRODUCTION AND TECHNICAL OVERVIEW

Photon-counting CT (PCCT) is a recently introduced CT technology that uses semiconductor detectors, such as cadmium telluride, cadmium zinc telluride, or silicon, in contrast to the energy-integrating detectors (EID) used in conventional CT scanners. These semiconductor detectors convert X-ray photons directly into electrical signals, whose pulse height is directly proportional to the energy of the X-ray photons (Fig. 1). Hence, each photon is allocated to a specific energy bin, and the detector can be programmed to count individual pulses that exceed a specific threshold [1]. The dual-source Naeotom Alpha (Siemens Healthineers), now known as Naeotom Alpha Peak, was the first PCCT to be approved by the FDA for commercial use. Other FDA-approved technologies include dual-source Naeotom Alpha Pro (Siemens Healthineers), single-source Naeotom Alpha Prime (Siemens Healthineers), a single-source PCCT by Canon Medical systems and a mobile OmniTom Elite PCCT (Neurologica, Samsung Electronics) [2]. Other vendors have prototypes at various stages of approval [3].

Unlike conventional EID CT, which has septa between the detectors to limit the diffusion of light, PCCT does not have septa. As a result, PCCT can have smaller detector elements of 0.151 x 0.176 mm, which allows for ultra-high-resolution (UHR) imaging with an in-plane spatial resolution of up to 0.11 mm [1]. UHR images were obtained using thin slices (e.g., 0.2 mm), sharp kernels (e.g., Bv56/68), and high matrices (e.g., 1,024 x 1,024). In PCCT, unlike EID-CT, UHR imaging does not require grid filters, which allows for geometric radiation dose efficiency.

PCCT has also improved spectral separation owing to multienergy binning. The quality of multienergy/spectral images is improved compared to that of EID-CT dual energy technologies because of the high temporal resolution of 66 ms and spatial and temporal registration due to spectral imaging at the detector level. In comparison, the dual-source EID-CT scan technology has a lower temporal resolution in the dual energy mode, and there is a 90° offset between the X-ray tubes and detectors. Spectral images include virtual monoenergetic images (VMIs), iodine maps, virtual non-contrast (VNC), and virtual non-calcium (VNCa) images. VMI

Received: March 16, 2024 **Revised:** November 24, 2025
Accepted: November 28, 2025
Corresponding author: Prabhakar Shantha Rajiah, MD, FRCR, Department of Radiology, Mayo Clinic, 200 1st Street SW, Rochester, MN 55902, USA
• E-mail: Rajiah.Prabhakar@mayo.edu

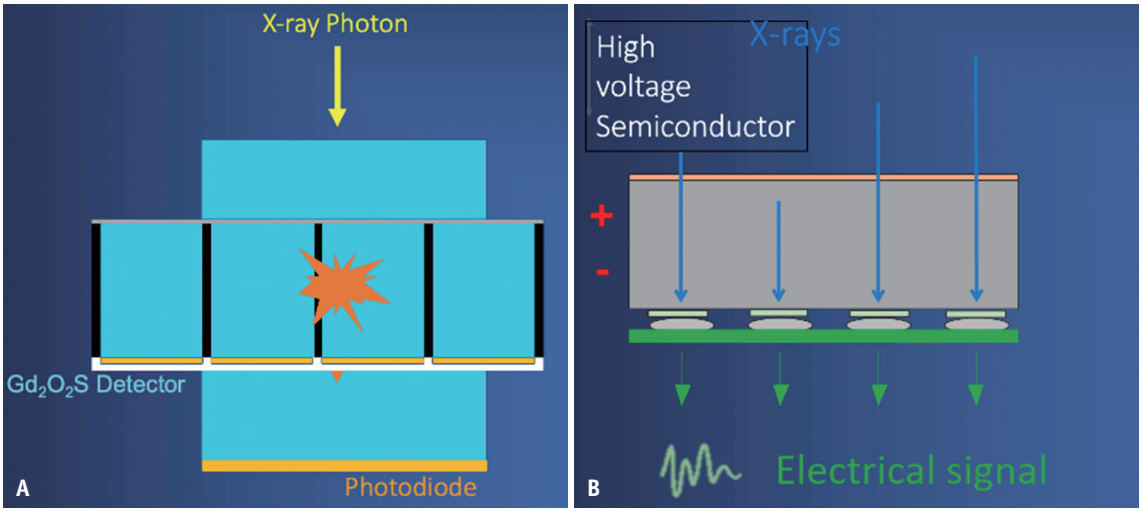

Fig. 1. PCCT scan technology. **A:** Schematic of a conventional energy-integrating detector CT scanner. An X-ray photon strikes a scintillator (e.g., gadolinium oxysulfide), which emits visible light (illustrated as a polygon). The light is then detected by a photodiode and converted into an electrical signal, resulting in a loss of information about the original photon during the intermediate light conversion. **B:** Schematic of a PCCT scanner. An X-ray photon strikes a semiconductor detector (e.g., cadmium telluride) and is directly converted into an electrical signal, the energy of which is proportional to that of the incoming photon. PCCT = photon-counting CT

mimics images obtained using a single-energy X-ray beam generated from 40 to 200 keV energy levels. VMI at 70 keV is equivalent to a conventional CT image, whereas VMIs <70 keV are labeled as low-energy and those >70 keV are labeled as high-energy. The attenuation of iodine increases in low-energy VMIs because photoelectric attenuation increases as the X-ray energy approximates the k-edge of iodine (i.e., 33 keV) [4]. Although traditional multi-energy techniques result in higher noise at low-energy levels which limits the lowest energy that can be used, PCCT has low noise even at low-energy levels. At the other end of the spectrum, high-energy VMI can reduce various artifacts including blooming, beam hardening, and metallic artifacts. Iodine maps and VNCs are generated using two-material decomposition (iodine and water). Iodine maps highlight iodine-containing pixels, whereas iodine-containing pixels are removed in VNC, which mimics true non-contrast (TNC) acquisition. PCCT also incorporates a novel three-material decomposition algorithm (iodine, water, and calcium) to generate virtual non-iodine (VNI; PURE Calcium, Siemens Healthineers) and VNCa (PURE Lumen, Siemens Healthineers) images. VNI preserves calcium more accurately than the traditional VNC. The VNCa removes calcium from the images.

Electronic noise is eliminated by using energy thresholds that exclude low-energy electronic noise [1,3]. This reduction improves image quality and enables the use of low-dose radiation protocols, which would otherwise be limited by noise. PCCT has an intrinsically high iodine contrast-to-noise ratio (CNR) owing to the equal weight of low-energy and high-energy photons [1,5,6].

In this article, we illustrate the clinical applications of PCCT in cardiovascular imaging using case examples from our institution with Naeotom Alpha (Table 1). The subsequent sections are organized according to the incremental value of PCCT in cardiovascular imaging. The sample protocols used in our institution are listed in Table 2.

IMPROVED ASSESSMENT OF DENSE CALCIFIED ARTERIES

A key limitation of EID-CT is its low accuracy in quantifying luminal stenosis caused by dense calcified plaques, particularly in small vessels. Although coronary CT angiography (CTA) has a high negative predictive value for the exclusion of obstructive coronary artery disease (CAD) and is the first-line test in low- to intermediate-risk populations [7], its accuracy and specificity decline in high-risk patients with extensive calcification [8]. Blooming artifacts from partial volume averaging exaggerate the extent of calcification, leading to overestimation of luminal stenosis and unnecessary referrals for invasive coronary angiography (ICA). Because partial volume averaging is a consequence of low spatial resolution, UHR imaging with PCCT reduces calcium blooming, enhances the definition of calcium, and improves the assessment of luminal stenosis (Fig. 2) [3]. A few studies, including those in high-risk cohorts, have

https://doi.org/10.3348/kjr.2024.0261

Korean Journal of Radiology
KJR

Table 1. Benefits of PCCT in cardiovascular imaging

Benefits	Image type	Comment
Improved assessment of dense calcified arteries	UHR: Decreased blooming ME: High-energy VMI ME: VNCa (PureLumen)	• Decreased calcium blooming improves assessment of luminal stenosis that correlates better with invasive angiography • Improved assessment of luminal stenosis by separation of calcium
Improved assessment of stents	UHR: Decreased blooming ME: High-energy VMI	• Improved visualization of stent structure • Decreased blooming improves assessment of in-stent stenosis that correlates better with invasive angiography
Improved visualization of vessels	UHR ME: Low-energy VMI	• Visualization of small vessels that are challenging in conventional CT helps in procedural planning • Use of low-dose iodinated contrast • Salvage of suboptimal enhanced studies
Improved assessment of vessel wall & plaque	UHR ME: VMI	• Enhances confidence of characterizing vessel wall and plaque. Potential for detecting novel risk factors
Material decomposition & characterization	Iodine map, VNC VNC, VNI (PureCalcium)	• Characterization of lesions that have similar attenuation in conventional images • Saves radiation dose of a true non-contrast acquisition
Myocardial assessment	VMI, Iodine map	• Myocardial perfusion, late iodine enhancement and extracellular volume are performed with higher image quality than EID-CT single and dual energy scans
Radiation dose reduction	VNC, VNI	• By eliminating a true non-contrast acquisition in some multiphasic studies and for calcium score in a patient who is getting a CT angiography
Combination of scan modes	Combined UHR/ME mode Combined Flash/ME mode	• Benefits of UHR and ME mode • Motion-free images with pulmonary perfusion maps and VMIs

PCCT = photon-counting CT, UHR = ultra-high-resolution, ME = multienergy, VMI = virtual monoenergetic image, VNCa = virtual non-calcium, VNC = virtual non-contrast, VNI = virtual non-iodine, EID = energy-integrating detector

demonstrated that the UHR mode correlates more accurately with quantitative ICA than with EID-CT [9-11]. Other studies have shown that PCCT reclassifies up to 54% of patients to a lower stenosis grade and CAD-RADS category compared with EID-CT, especially in cases of calcified and partially calcified plaques (Fig. 2A, B) [9-12]. Consequently, CTA can now be applied more reliably in high-risk populations, including patients undergoing evaluation for transcatheter aortic valve replacement (TAVR) [13]. Recent studies further indicated that PCCT reduces unnecessary ICA referrals and other downstream tests, lowering healthcare costs while increasing the rate of appropriate revascularization [14,15].

Beyond the coronary arteries, PCCT also improves the assessment of luminal stenosis in lower-extremity runoff vessels, particularly in small arteries below the knee. In these arteries, it is difficult to distinguish between calcium and contrast, resulting in both over- and under-estimation of stenosis on EID-CT. As a result, CTA accuracy is lower for below-knee vessels than for the proximal arteries with EID-CT. Various EID-CT techniques have been employed to mitigate this problem, including delayed acquisition, calcium subtraction using non-contrast imaging, and dual-energy calcium separation [16]. UHR with PCCT enhances calcium definition, reduces blooming, and improves stenosis assessment [17]. This translates into greater arterial sharpness, higher diagnostic confidence, reduced uncertainty, and fewer misclassified segments as occluded (Fig. 2C, D) [16].

Spectral imaging can also improve the evaluation of densely calcified lesions. High-energy VMI is another effective method for mitigating blooming by decreasing the average attenuation of the materials in a voxel. High-energy VMI improves stenosis evaluation and correlates more closely with ICA than with conventional imaging [18,19]. High-energy VMI also decreases the beam-hardening artifacts, which appear as dark streaks owing to the preferential attenuation of low-energy photons. VMIs at energies >100 keV are particularly effective in decreasing these artifacts [20]. However, as the iodine signal decreases at higher energies, it is essential to review lower-energy

 https://doi.org/10.3348/kjr.2024.0261

Table 2. Sample PCCT cardiovascular protocols in our institution

	Coronary CTA-UHR	Coronary CTA-ME	Thoracic aortic CTA
Scan range	• Carina to bottom of heart • Entire heart for bypass grafts	• Carina to bottom of heart • Entire heart for bypass grafts	• Lung apices-bottom of heart
Bolus track	Ascending aorta at level of pulmonary artery	Ascending aorta at level of pulmonary artery	Ascending aorta at level of pulmonary artery
Scan mode	Spiral	Spiral/sequential/flash	
Direction	Craniocaudal	Craniocaudal	Craniocaudal
CARE Dose4D	Yes	Yes	Yes
CARE keV optimization target	Vascular	Vascular	Vascular
Tube voltage, kVp	90 or 120	120	120
CARE keV IQ level	100 (90 kV) or 50 (120 kV)	50	50
Collimation, mm	120 x 0.2	144 x 0.4	144 x 0.4
Pulsing mode	Standard	Standard for spiral; manual for sequential	• Gated Flash (≤75 bpm and regular, Pt width <45 cm) • Gated sequential (too large for Flash mode) • Non-gated flash • Gated spiral mode • Non-gated Spiral mode
Phase start/end	40%–75%	40%–75% for spiral, 65%–75% for sequential; 55% for flash	65%
Kernels	Bv60	Bv48	Bv44, Bv56
QIR strength	4	4	4
Standard recon	Conventional images (T3D)	Monoenergetic plus-70 keV	Monoenergetic plus-70 keV
Spectral recons	None	50 keV Bv48 Iodine map Qr40 VNC Qr40 PureLumen Bv48 SPP Qr40	50 keV Bv48 Iodine map Qr40 VNC Qr40 PureLumen Bv48 SPP Qr40
Recon phases	Best diastolic, best systolic, multiphase 0%–95% at 5% increments	Best diastolic, best systolic, multiphase 0%–95% at 5% increments in spiral mode	Sequential: single best phase (70% or 200–400 ms at HR >85 bpm or irregular)
Slice thickness, mm	0.2	0.4	1.0
Increment, mm	0.1	0.3	0.5
Matrix size	1,024 x 1,024	Auto	Auto

PCCT = photon-counting CT, CTA = CT angiography, UHR = ultra-high-resolution, ME = multienergy

images as well for optimal lumen visualization [3]. Spectral calcium separation is another technique that can reduce calcium blooming. VNCa images subtract calcium from the images, making calcium appear grayish instead of white (Fig. 3). As a result, it is easier to distinguish gray-colored calcium from white-colored contrast-enhanced coronary arterial lumen. This improves the assessment of luminal stenosis, which correlates better with ICA [21,22]. However, occasional erroneous plaque subtraction can result in false-positive or false-negative diagnoses in up to 12% of cases [22]. VNCa also enhances the assessment of calcified plaques in peripheral runoff arteries. In one study, sensitivity, specificity, and accuracy for stenosis detection compared with digital subtraction angiography were 85%, 89%, and 88%, respectively, slightly lower than conventional imaging (91%, 95%, and 93%) [17]. In addition, bone-subtraction algorithms based on material decomposition are faster and more robust than traditional threshold-based approaches [4].

IMPROVED ASSESSMENT OF STENTS

The evaluation of stents, particularly small stents, remains a challenge with EID-CT because blooming artifacts obscure both the stent structure and the underlying lumen.

https://doi.org/10.3348/kjr.2024.0261

Korean Journal of Radiology
KJR

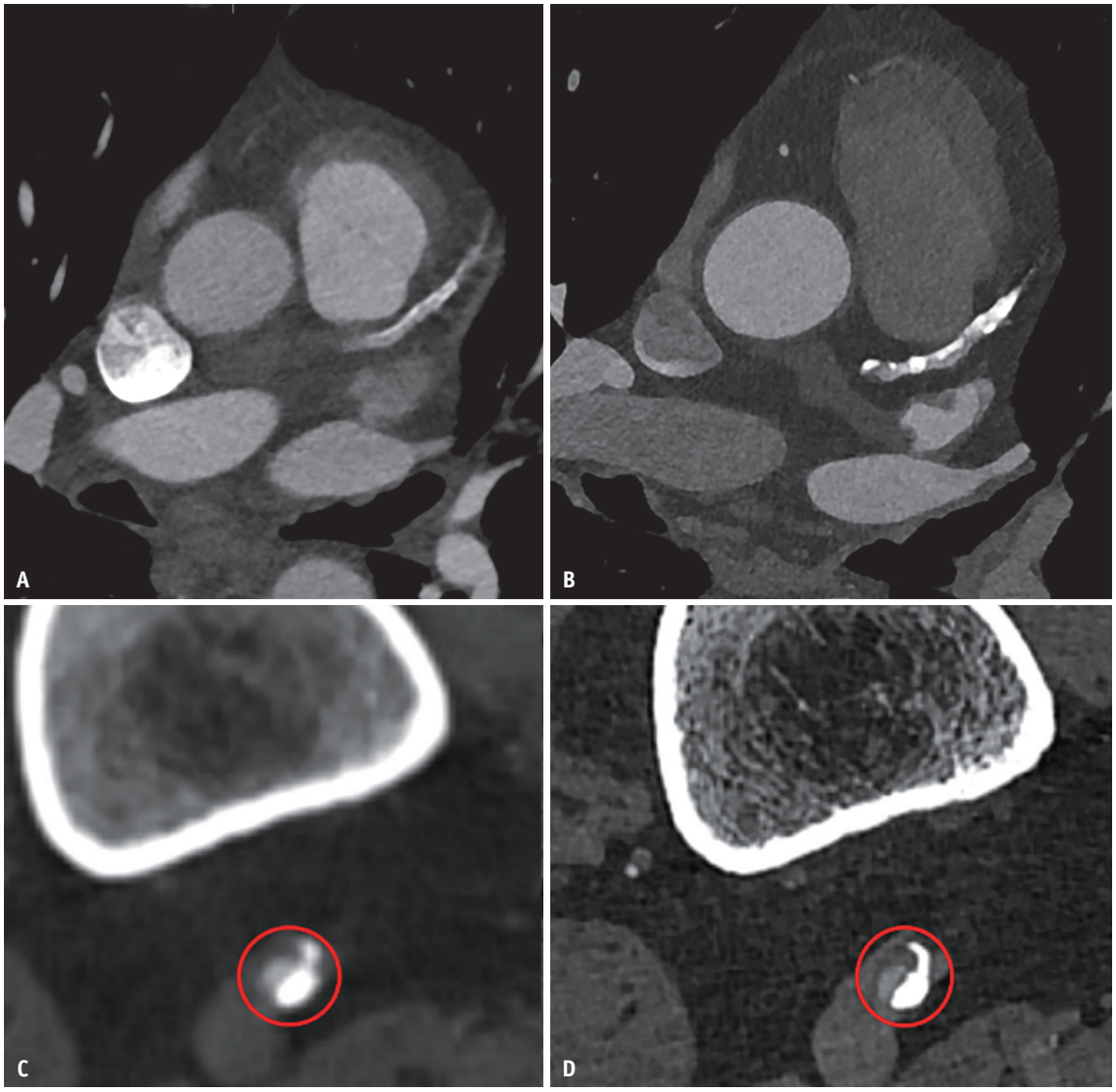

Fig. 2. Improved assessment of dense calcified arteries. **A:** Axial oblique coronary CTA from an EID-CT scanner in a 71-year-old male shows dense calcified plaque in the proximal and mid left anterior descending coronary artery, resulting in severe stenosis. Calcium margins are poorly defined. **B:** Coronary CTA in the same patient from a PCCT scanner shows sharper plaque definition with reduced blooming, revealing moderate stenosis. By reducing blooming, PCCT enables more accurate estimation of luminal stenosis, which correlates more closely with invasive coronary angiography. **C:** Axial CTA in a 75-year-old male shows a heavily calcified popliteal artery with severe stenosis and marked calcium blooming on EID-CT (red circle). **D:** Axial CTA in the same patient from PCCT shows sharper plaque definition, reduced blooming, and improved assessment of stenosis (red circle). CTA = CT angiography, EID = energy-integrating detector, PCCT = photon-counting CT

Consequently, CTA is recommended only for stents larger than 3 mm in diameter and with a strut thickness >100 μm [23]. PCCT UHR imaging decreases stent blooming and enhances the visualization of stent architecture, including luminal assessment of neointimal hyperplasia and in-stent restenosis [24]. Several studies have demonstrated the advantages of PCCT in coronary stent imaging, particularly when using sharp reconstruction kernels (e.g., Bv72), thin slices, and high temporal resolution (Fig. 4A, B) [25-28]. These benefits also extend to small stents [28]. PCCT improves diagnostic accuracy in detecting neointimal hyperplasia, with stenosis assessment showing a strong correlation with ICA findings [9,25,26]. Beyond the coronary circulation, PCCT has also proven valuable for evaluating small stents in other vascular territories, including the renal arteries and stents used in fenestrated endovascular aortic repair (Fig. 4C, D). Similar to dense calcified plaques (discussed above), high-energy VMIs (>100 keV) can also decrease blooming, beam hardening,

 https://doi.org/10.3348/kjr.2024.0261

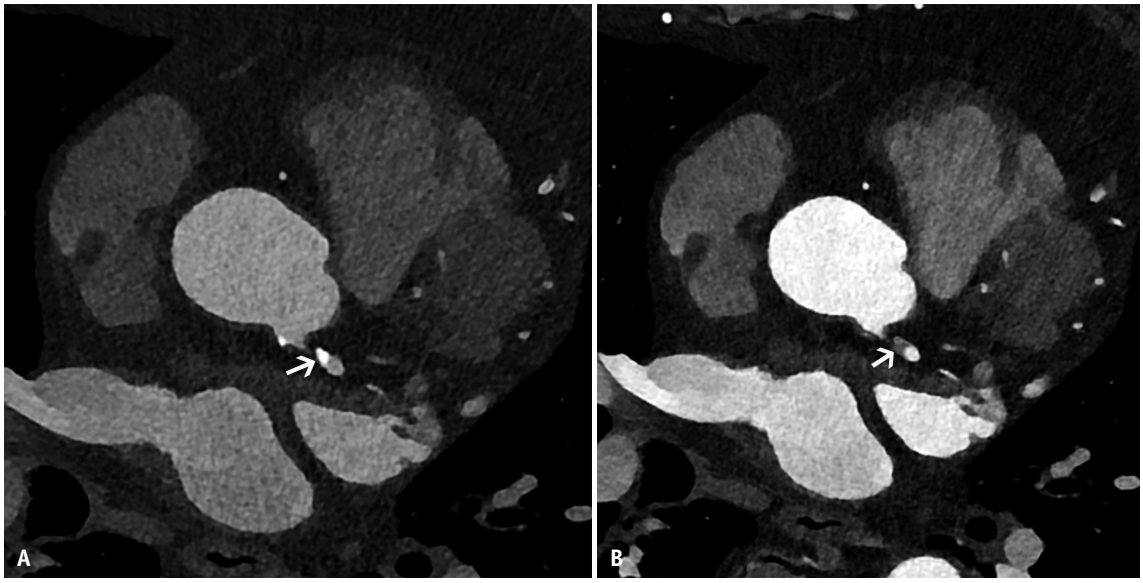

Fig. 3. Material-based calcium separation. **A:** Coronary CT angiography from photon-counting CT in a 75-year-old female shows dense calcified plaque in the left main coronary artery (arrow) with moderate stenosis. **B:** Virtual non-calcium reconstruction (PureLumen) using a three-material decomposition algorithm replaces calcium pixels with gray color (arrow), mitigating the effect of calcium blooming and improving stenosis assessment.

and metallic artifacts near stents [20].

IMPROVED VISUALIZATION OF VESSELS

The evaluation of small vessels can be significantly improved in PCCT by using both UHR and spectral capabilities. The UHR capabilities of PCCT enhance the visualization of small vessels beyond what is possible with EID-CT. In the coronary arteries, PCCT improves the delineation of the small side branches. CAD-RADS requires assessment of all coronary artery branches >1.5 mm; improved visualization with PCCT may prompt future updates to include smaller branches [6]. Beyond the coronaries, PCCT improves the assessment of the digital arteries in the hand, providing valuable information for evaluating ischemic conditions such as thromboangiitis obliterans and scleroderma. Similarly, the improved depiction of small vessels in the foot supports advances in peripheral vascular interventions and surgery, allowing for interventional procedures in the distal vessels. Identification of the artery of Adamkiewicz, which is critical for spinal cord perfusion in thoracoabdominal aortic surgery, remains challenging using EID-CT, often requiring large contrast volumes, precise timing, and delayed acquisition. PCCT facilitates reliable identification at low-contrast doses [29]. PCCT also enhances the visualization of the perforator arteries for reconstructive surgery, demonstrating more perforators, improved depiction of smaller branches, and a clearer anatomic definition [16,30]. It is similarly useful for mapping the prostatic branches for prostate artery embolization and inferior rectal branches for rectal artery embolization [31]. Improved visualization of tumor-involved small vessels enhances surgical planning and supports 3D modeling and printing for preoperative assessment of cardiac tumors (Fig. 5). Overall, the improved definition of small vessels by using PCCT may reduce the number of surgical and interventional procedures required.

The high-iodine CNR of PCCT and low-energy VMIs can also improve the visualization of small vessels. These properties can also be leveraged with a low dose of an iodinated contrast agent, especially in patients with severe renal dysfunction. The high iodine signal in low-energy VMI can also be used to rescue suboptimally enhanced studies without the need to repeat the scan on a conventional EID-CT scanner, which leads to increased contrast and radiation doses, as well as patient discomfort and dissatisfaction. Multiple studies have demonstrated the value of low-energy VMI (40, 50, or 55 keV) in reducing contrast doses in CTA by up to 50% (Fig. 6) [32-34].

IMPROVED ASSESSMENT OF VESSEL WALL AND PLAQUE

The UHR capabilities of PCCT also allow the comprehensive evaluation of the vessel wall in conditions such as vasculitis,

https://doi.org/10.3348/kjr.2024.0261

Korean Journal of Radiology
KJR

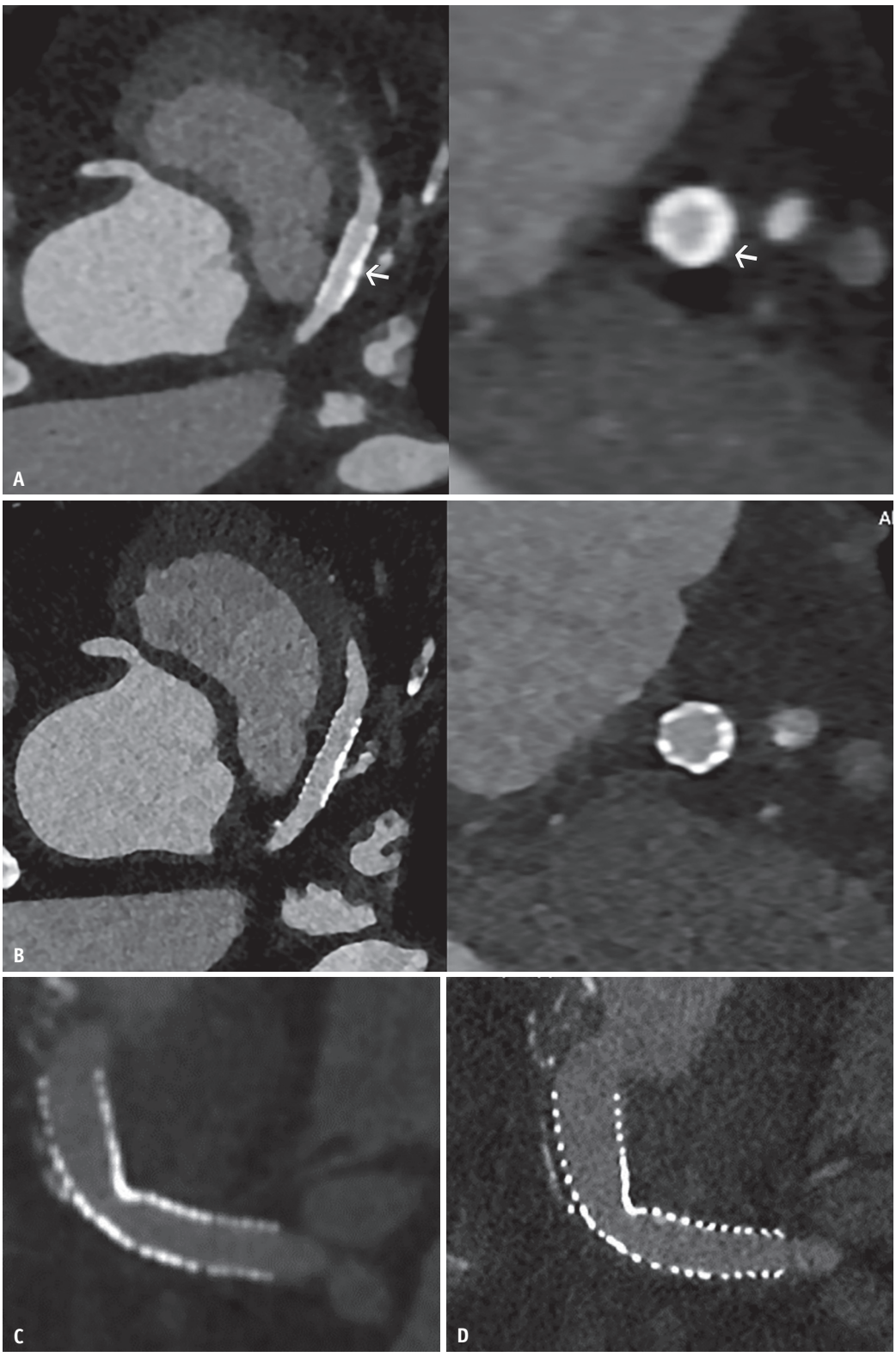

Fig. 4. Improved evaluation of stents. **A:** Axial oblique (left) and short-axis (right) coronary CTA in a 64-year-old male from an EID-CT scanner shows a proximal left anterior descending coronary artery stent (arrows) with poor strut definition due to blooming artifact. **B:** Coronary CTA in the same patient from PCCT (left = oblique axial; right = short-axis) shows sharper stent definition, reduced blooming, and improved visualization of stent struts and lumen. **C:** Coronal oblique CTA in a 55-year-old female from EID-CT shows poor definition of a renal artery stent. **D:** Coronal oblique CTA in the same patient from PCCT shows sharper stent margins, reduced blooming, and improved luminal assessment. CTA = CT angiography, EID = energy-integrating detector, PCCT = photon-counting CT

https://doi.org/10.3348/kjr.2024.0261

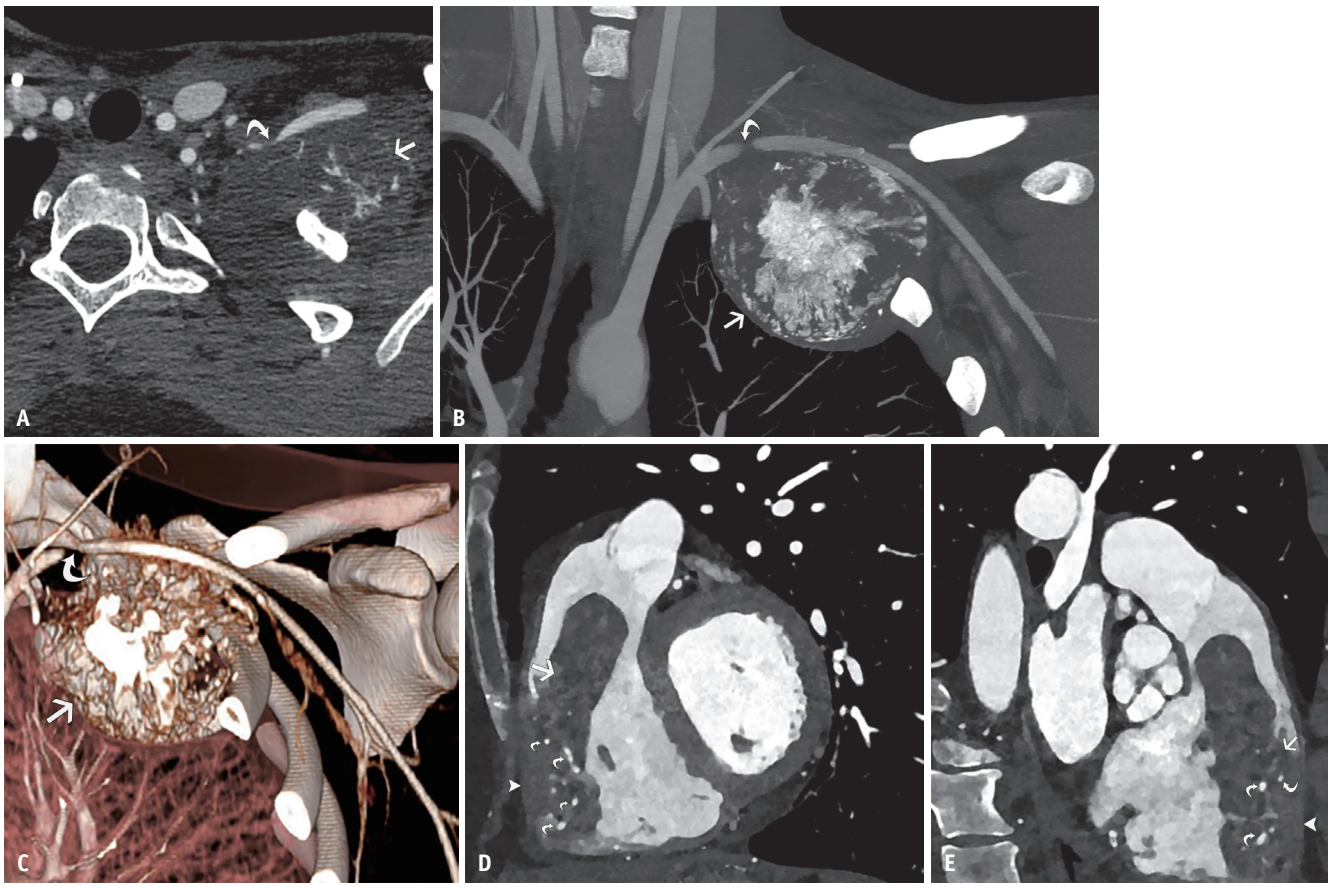

Fig. 5. Improved visualization of small vessels. **A-C:** Axial CTA **(A)**, coronal MIP image **(B)** and 3D-volume rendered construction **(C)** from PCCT in a 16-year-old male with osteosarcoma of the first rib demonstrates the mass (arrows) which abuts and severely narrows the left subclavian artery (curved arrows). The tumor was resected, and a graft restored patency. **D:** Sagittal oblique CTA from PCCT in a 63-year-old male with metastatic hepatocellular carcinoma in the RV shows a mass (arrow) narrowing the RV outflow tract, infiltrating the RV free wall (arrowhead), and supplied by small marginal RCA branches (curved arrows). **E:** Coronal oblique CTA in the same patient shows the mass (arrow), RV wall infiltration (arrowhead), and feeding marginal branches (curved arrows). CTA = CT angiography, MIP = maximal intensity projection, PCCT = photon-counting CT, RV = right ventricle, RCA = right coronary artery

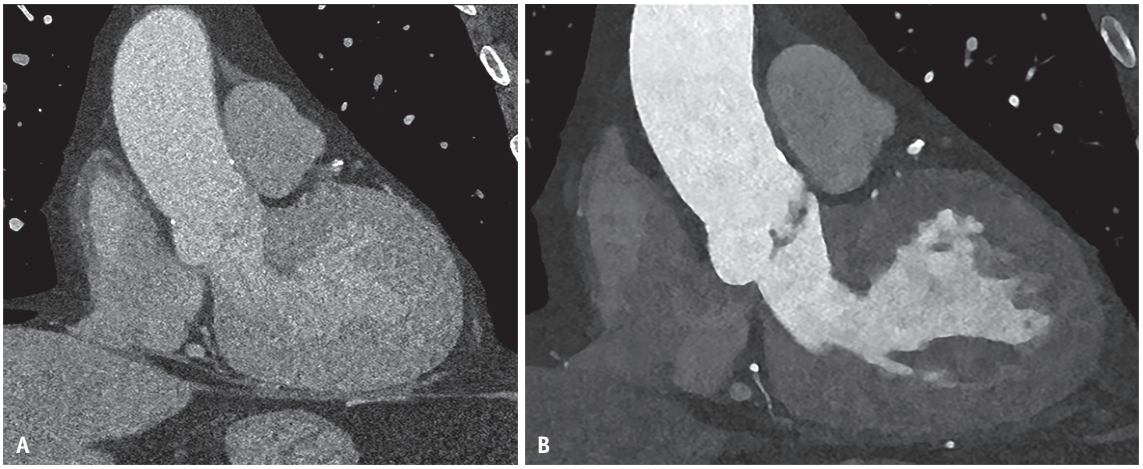

Fig. 6. Salvage of suboptimally enhanced CTA using multienergy technique. **A:** Coronal oblique CTA from photon-counting CT in a 75-year-old male shows suboptimal aortic opacification (mean, 191 HU) due to contrast extravasation during the scan. **B:** Coronal oblique 50-keV image in the same patient shows improved iodine signal (mean, 450 HU). Low-keV virtual monoenergetic image enhances iodine conspicuity, allowing for a reduced contrast dose and salvaging suboptimally enhanced studies. CTA = CT angiography, HU = Hounsfield unit

https://doi.org/10.3348/kjr.2024.0261

Korean Journal of Radiology
KJR

fibromuscular dysplasia (FMD), and atherosclerotic plaques. Florid vasculitis is typically evident on EID-CT as mural thickening, enhancement, and perivascular stranding; however, early or subtle diseases may be difficult to detect. PCCT improves the sensitivity to these subtle changes. Similarly, while classic FMD is identified by beaded irregularities of alternating stenoses and aneurysms, PCCT better depicts early or subtle wall abnormalities, often challenging to detect with EID-CT [6]. Plaque quantification and characterization are emerging as key tools for risk stratification and personalized therapy. High-risk plaque features, including low attenuation (<30 Hounsfield unit [HU]), spotty calcification, napkin-ring sign, and positive remodeling, are associated with adverse cardiovascular outcomes, with low-attenuation plaques carrying the highest risk [35]. A greater total plaque volume and a higher volume of individual plaque components are also associated with poor outcomes [35]. PCCT at UHR improves the delineation

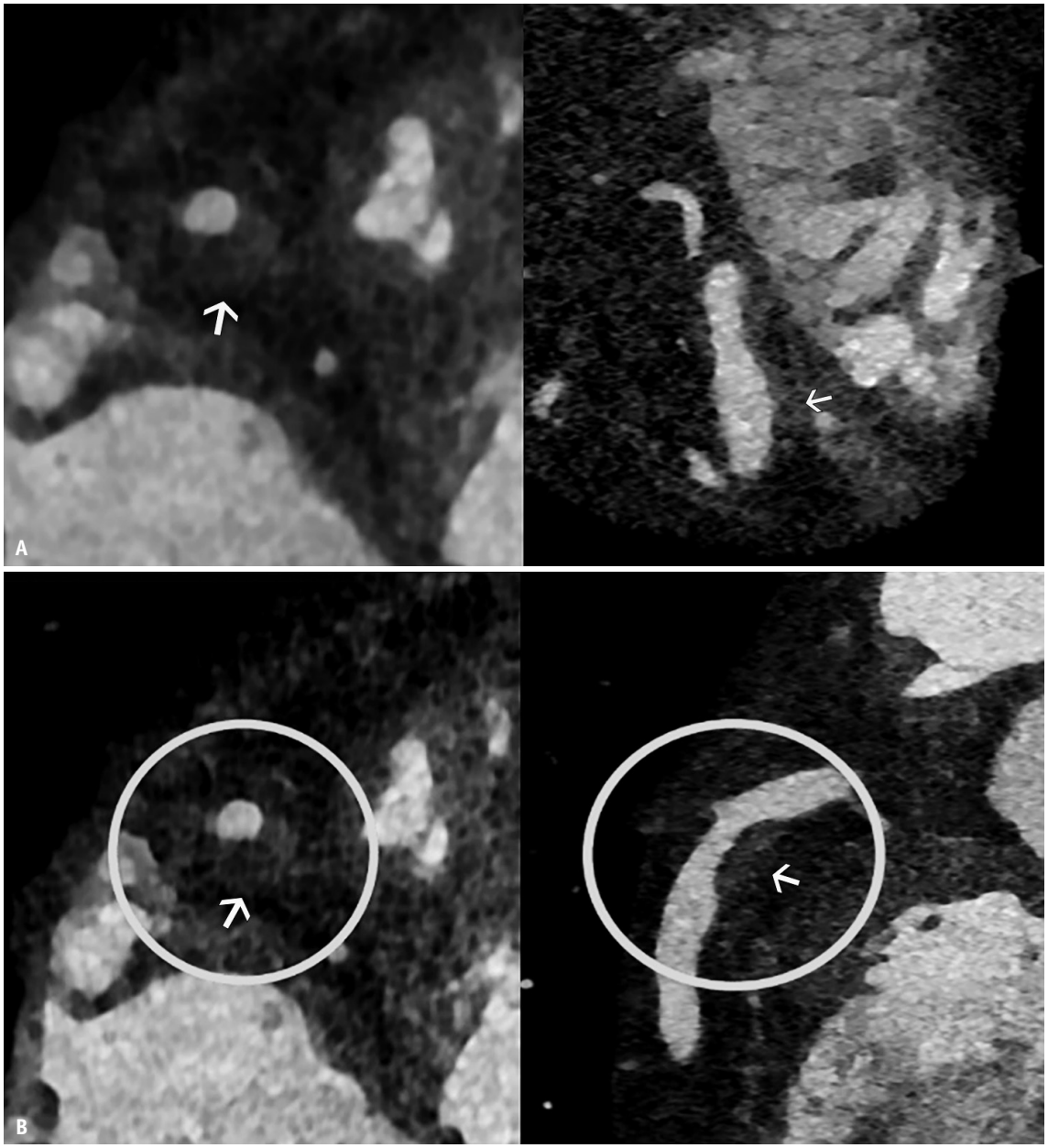

Fig. 7. Vessel wall and plaque characterization. **A:** Short-axis and axial oblique CTA from an energy-integrating detector-CT in a 61-year-old female shows a non-calcified plaque in the mid right coronary artery with positive remodeling (arrows), causing mild stenosis. **B:** CTA from photon-counting CT in the same patient shows improved plaque definition with clear visualization of a central low-attenuation lipid core (arrows), indicating a high-risk plaque prone to rupture. CTA = CT angiography

https://doi.org/10.3348/kjr.2024.0261

of plaque components and may help identify novel risk markers (Fig. 7). Importantly, different thresholds may be required for plaque quantification with PCCT compared to EID-CT. Several studies have shown that UHR decreases calcified plaque volume (due to reduced blooming) and increases non-calcified, low-attenuation plaque volume (due to improved image quality), resulting in up to a 33% reduction in measured total plaque volume [36,37].

Plaque analysis is typically performed by categorizing plaques into calcified, fibrotic, or lipid-rich components based on CT attenuation thresholds, which vary with tube potential and patient size. Spectral imaging with VMIs improves reproducibility by standardizing attenuation values across different energy levels [38]. PCCT also improves coronary artery calcium scoring (CACS). One study demonstrated that CACS is lower with PCCT by approximately 4% due to reduced blur artifacts [39], whereas another found higher scores than EID-CT, attributed to reduced partial volume averaging and detection of more voxels above the 130 HU threshold [18]. Using VMI, the CACS on 70-keV PCD-CT is lower than that on EID-CT [19], and scores further decrease with higher keV levels and greater iterative reconstruction strength [40].

MATERIAL DECOMPOSITION & CHARACTERIZATION

Spectral images, including iodine maps and VNC, are valuable for lesion characterization, including incidentally detected findings (Fig. 8). A common application is the evaluation of cardiac masses, particularly the differentiation of thrombi from neoplasms or slow-flow artifacts. Conventional CT relies on attenuation values, delayed imaging, or prone positioning, whereas PCCT iodine maps provide direct quantification. Thrombi demonstrate absent or very low iodine signals, whereas slow-flow regions contains measurable iodine. A threshold of <1.74 mg/mL has been shown to yield 100% sensitivity and specificity (area under curve = 1) in distinguishing thrombi from slow flows [4,41], although cutoffs specific to PCCT have not yet been established. Neoplasms typically demonstrate a higher iodine content, allowing distinction from thrombi. The combination of iodine maps, VNC, and VNCa reconstructions can further aid in lesion characterization. For incidentally detected hyperattenuating lesions, the VNC distinguishes between iodine-related enhancement and other causes of hyperdensity. The persistence of hyperattenuation on the VNC suggests hemorrhage, calcium, or surgical material, whereas its persistence on the VNCa specifically indicates hemorrhage. The presence of iodine on iodine maps indicates enhancement or active bleeding [4].

CACS can be calculated from the VNC derived from CTA, eliminating the need for separate TNC acquisition, thus reducing radiation exposure. Although the VNC-derived CACS correlates with TNC-derived scores, the values are not identical [3]. VNI has been shown to have closer agreement with CACS from TNC than with VNC (r = 0.97) (Fig. 9) [41-45]. Small or low-density plaques may be missed on standard VNI at 70 keV; however, using safety-net reconstructions with 55 keV VNI, iterative reconstruction (level 2), and a 110 HU threshold can improve detectability, preventing erroneous CAC scores of zero in approximately 18% of patients [46].

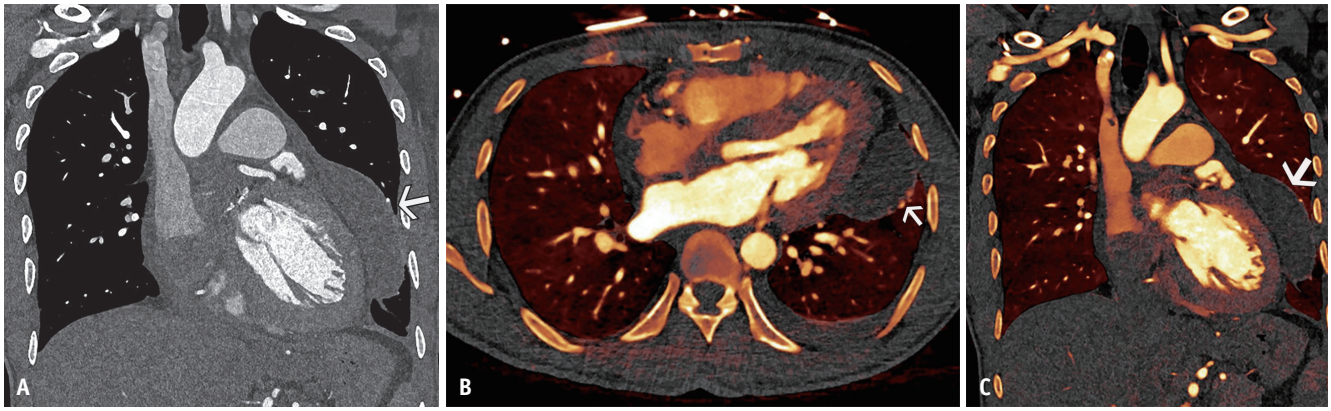

Fig. 8. Multienergy characterization of incidental lesion. **A:** Coronal oblique CT angiography in a 42-year-old male post-Bentall procedure, subaortic resection, Konno root enlargement, and tricuspid annuloplasty shows a complex hyperattenuating mediastinal hematoma (arrow). **B, C:** Axial **(B)** and coronal **(C)** iodine maps in the same patient show absence of iodine in the lesion (arrows), confirming the lesion as a postoperative seroma.

https://doi.org/10.3348/kjr.2024.0261

Korean Journal of Radiology
KJR

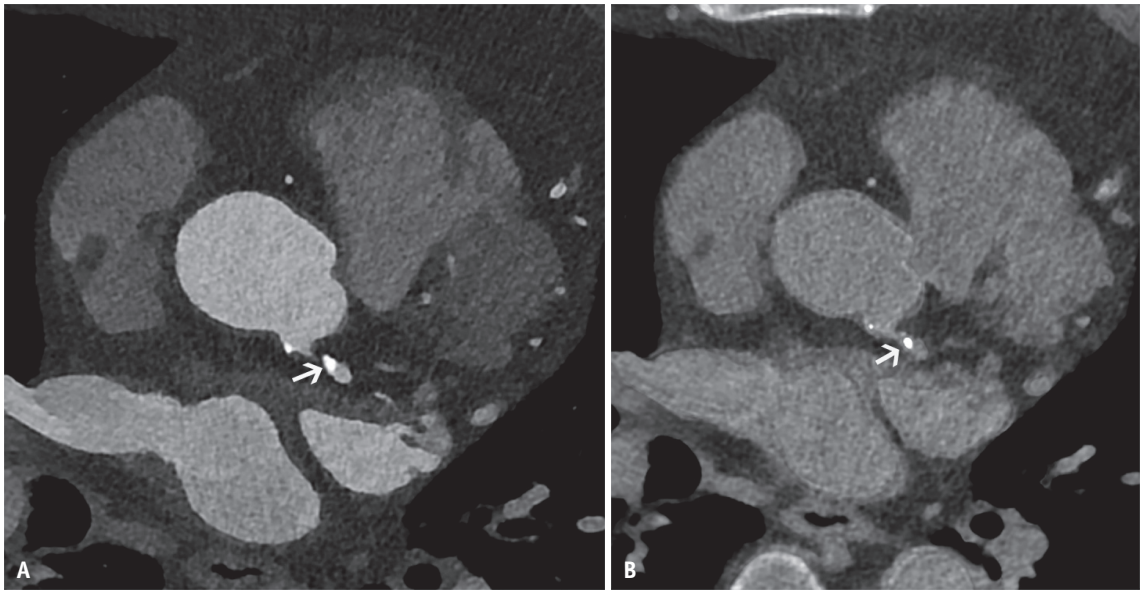

Fig. 9. Calcium scoring from virtual non-iodine image. **A:** Coronary CT angiography from photon-counting CT in a 75-year-old female shows dense calcified plaque in the left main coronary artery (arrow) with moderate stenosis. **B:** Virtual non-iodine reconstruction (PURE Calcium) subtracts iodine but retains calcium (arrow), enabling calcium scoring without acquiring a separate non-contrast CT scan, thus reducing radiation exposure.

MYOCARDIAL ASSESSMENT

The improved spectral performance of PCCT enhances the myocardial perfusion imaging, late iodine enhancement (LIE), and extracellular volume (ECV) quantification. Although these techniques can be performed using conventional EID-CT, PCCT provides superior image quality and diagnostic performance [3,47,48]. Myocardial perfusion can be assessed qualitatively using iodine maps and VMIs and quantitatively with dynamic acquisitions. Low-energy VMIs and iodine maps improve the sensitivity for detecting subtle perfusion defects, whereas high-energy VMIs reduce beam-hardening artifacts in the subendocardial regions adjacent to the left ventricle blood pool, thereby improving specificity [4]. In one study, PCCT myocardial perfusion imaging demonstrated 100% positive predictive value for diagnosing myocardial ischemia using ICA or MRI as the reference standard [49].

LIE imaging, acquired 3–10 minutes after contrast administration, allows the evaluation of myocardial scars as an alternative to MRI, supporting the diagnosis of cardiomyopathy and risk stratification. EID-CT is limited by a low CNR, but PCCT, with lower noise, higher spatial resolution, and spectral imaging, significantly improves LIE quality (Fig. 10) [50]. In a canine model, PCCT enabled the simultaneous discrimination of gadolinium and iodine administered at different time points using dedicated material maps. In this setting, iodine was used to assess the coronary anatomy and lesions, whereas gadolinium was used to delineate the myocardial scar [51].

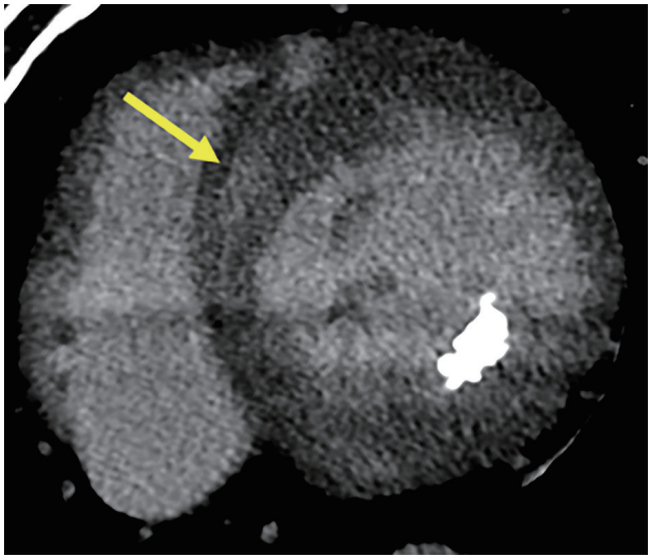

Fig. 10. Myocardial assessment. Short-axis 50-keV virtual monoenergetic image from photon-counting CT in a 51-year-old male with hypertrophic cardiomyopathy shows patchy mid-myocardial late iodine enhancement in the basal anteroseptum (arrow).

PCCT can also quantify the myocardial ECV by measuring iodine attenuation in the myocardium and blood pool on delayed contrast-enhanced scans combined with either a measured or synthetic hematocrit. Radiation exposure is reduced by deriving values from iodine maps and the VNC

https://doi.org/10.3348/kjr.2024.0261

rather than acquiring a TNC dataset. ECV mapping has been applied for the incidental diagnosis of cardiac amyloidosis during TAVR evaluation, which is an adverse prognostic factor [52]. Studies have shown a strong correlation between PCCT-derived and MRI-derived ECV in various populations, including patients with pre-TAVR and myocarditis [53-56].

RADIATION DOSE REDUCTION

PCCT offers several options to reduce the radiation dose in CT scans. The inherent low electronic noise allows the use of lower-radiation-dose which are traditionally limited by increased noise. The absence of reflective septa allows geometric dose efficiency even in UHR mode, unlike EID-CT, where grid filters are used. Multiphasic vascular studies such as those for post-EVAR evaluation typically require non-contrast, arterial, and venous phase acquisitions. Non-contrast acquisition is required to distinguish calcium from active bleeding, arterial phase acquisition is required for stent assessment and arterial endoleaks, and venous phase acquisition is required for delayed endoleaks. With PCCT, a VNC can potentially replace a TNC scan, and a low-energy VMI can replace the arterial phase. In addition to single delayed-phase acquisition, virtual arterial phase images can

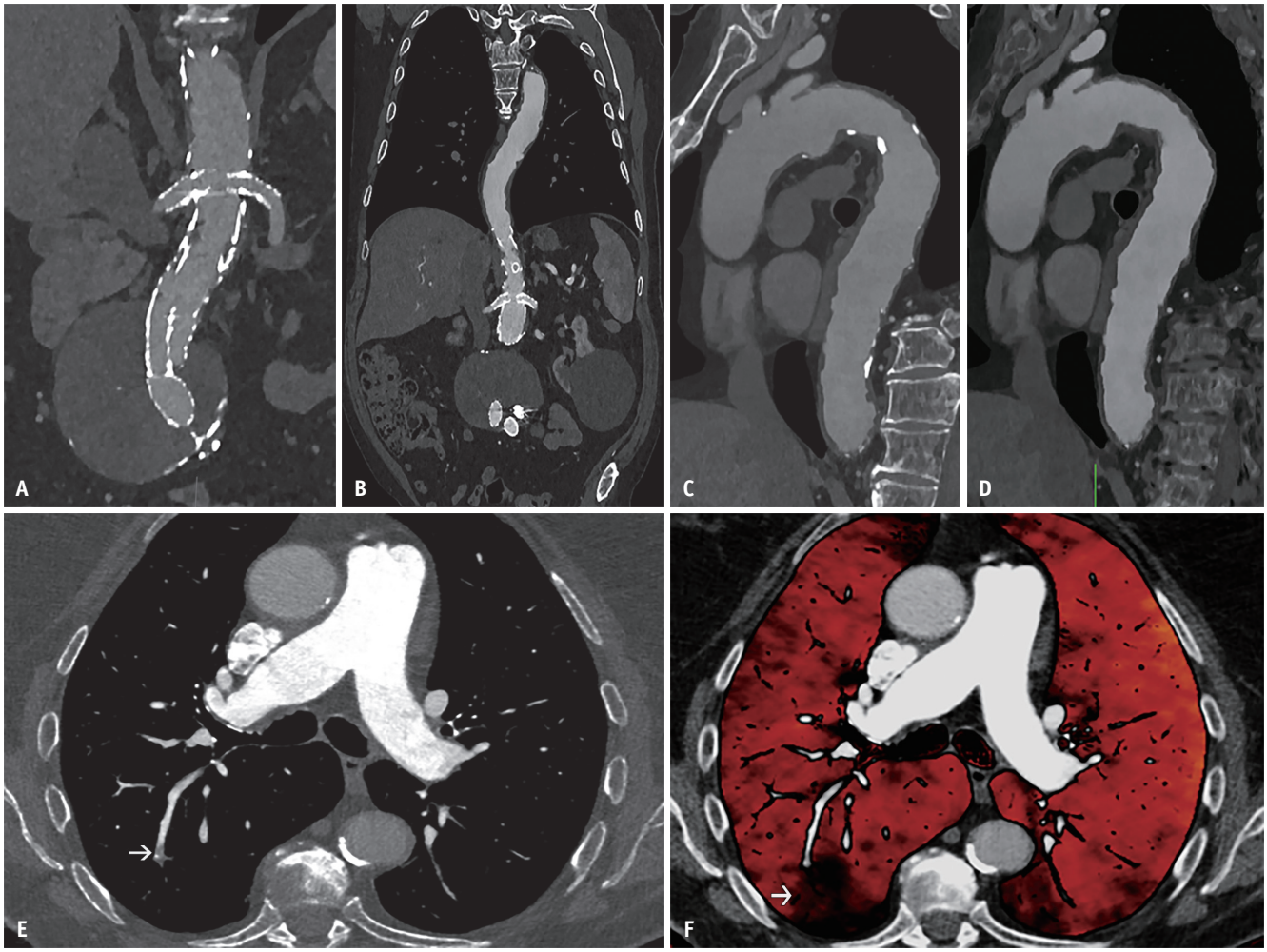

Fig. 11. Combined PCCT modes. **A:** Coronal oblique CTA from PCCT in UHR-ME mode in an 81-year-old male post-fenestrated endovascular aortic repair shows sharp definition of the stent structure, including renal artery stents. **B:** ME reconstruction in the same patient (50 keV) shows enhanced contrast visualization. **C:** Sagittal oblique UHR image shows calcified descending thoracic aortic plaque. **D:** PureLumen reconstruction shows calcium separation with reduced blooming. **E:** Axial CTA from PCCT in Flash-ME mode in 43-year-old male shows motion-free pulmonary arteries with embolus in the posterior segmental right lower lobe branch (arrow). **F:** Iodine map in the same patient shows a corresponding perfusion defect (arrow). Flash-ME mode enables simultaneous motion-free imaging of the coronary, aortic, and pulmonary arteries, along with ME maps (iodine, virtual monoenergetic image). PCCT = photon-counting CT, CTA = CT angiography, UHR = ultra-high-resolution, ME = multienergy

https://doi.org/10.3348/kjr.2024.0261

Korean Journal of Radiology
KJR

also be generated using low-energy VMI along with VNC, allowing one-third of the radiation dose compared with a conventional three-phase protocol [57].

COMBINATION OF SCAN MODES

PCCT offers several combined and novel scanning modes for cardiovascular imaging. In the early developmental stages of the scanner, a choice had to be made between the UHR and ME modes; however, a combined UHR/ME mode is now available, including in gated cardiac CT studies (Fig. 11A-D). This allows the concomitant acquisition of UHR and ME images, providing excellent quality for cardiovascular imaging. The development of novel contrast agents may further improve plaque characterization and provide novel biomarkers. An animal study using gold nanoparticles showed effective localization of nanoparticles in inflamed and unstable coronary plaques using gold images and UHR capabilities [58]. However, the collimation of this combined mode for gated studies is only 96 x 0.2 mm, compared with 120 x 0.2 mm for UHR mode and 144 x 0.4 mm for the ME standard-resolution mode.

Similarly, combined high-pitch helical (Flash) and multienergy modes are available. This mode is not available in dual-source EID-CT; as a result, a choice must be made between Flash and ME modes, i.e., between the need for motion-free images and perfusion maps or low-energy VMI for contrast. This choice is not required with the PCCT scanner. As a result, motion-free images of the pulmonary arteries, aorta, and coronary arteries can be obtained, along with iodine maps and VMIs that facilitate low-dose contrast studies (Fig. 11E, F) [59,60].

CHALLENGES IN CLINICAL APPLICATION

In addition to the higher costs, there are a few challenges in the implementation of PCCT in routine clinical practice (Table 3). The implementation of PCCT as a novel technology for cardiovascular imaging in clinical practice involves a steep learning curve. PCCT has several scan modes (UHR, ME, UHR + ME), acquisition techniques (spiral, axial, high-pitch spiral), kernels (Bv, Br, Qr at varying strengths), quantum iterative reconstruction strengths, slice thicknesses, matrices (512 x 512 or 1,024 x 1,024), and tube voltages (70 to 140 kVp). The generated spectral images can vary depending on the scan mode and tube voltage. A new automated radiation dose technique called CAREkEV has been used instead of CAREkVp [3]. Radiologists and technologists should be aware of these parameters to optimize them for specific clinical indications. Contrast injection protocols must

Table 3. Challenges of PCCT

Challenge	Comment	Solution
Cost	Significantly higher than EID-CT	• Potentially will decrease with time and competition from other vendors
Steep learning curve	Multiple scan modes, acquisition techniques, kernels, iterative reconstruction strengths, slice thickness, matrix, tube voltages, spectral images, automated dose modulation	• Knowledge sharing from experts and education of radiologists and technologists
Noise	Although electronic noise is low in PCCT, it can increase with sharp kernels, thin slices and higher matrix used in UHR mode	• Optimal selection of patients- limiting large patients for UHR mode • Selection of optimal kernel • Increase iterative reconstruction level or noise reduction techniques including artificial intelligence
Smaller collimation	The UHR mode and UHR/ME mode have smaller collimations than standard resolution/ME mode Increased probability of motion artifacts	• Utilization of UHR mode in appropriate patients • Optimize contrast protocol for a longer scan time
Artificial looking images	Edge correction algorithms in some of the vascular kernels	• Use sharper kernels
Increased data	Significantly increase data transfer time from scanner to PACS Increased storage requirements	• Optimize the protocols to acquire only necessary images • Create additional storage

PCCT = photon-counting CT, EID = energy-integrating detector, UHR = ultra-high-resolution, ME = multienergy, PACS = Picture Archiving and Communication System

 https://doi.org/10.3348/kjr.2024.0261

be modified for specific scanning modes. The UHR modes have smaller collimations (120 x 0.2 mm for UHR, 96 x 0.2 mm for UHR/ME mode), which require a longer contrast bolus for adequate opacification and a spiral acquisition to avoid the prolonged scan duration of sequential mode.

The high spatial resolution of the UHR mode comes at the expense of higher image noise (Fig. 12A, B). Hence, the UHR mode is not suitable for large patients. The mitigation of noise in the UHR mode requires optimization of the kernel and the use of noise-reduction algorithms, including those that are based on deep learning. The standard-resolution ME mode is suitable for large patients to optimize image quality at lower noise levels without excessive radiation exposure [3]. Additionally, low-energy VMI boosts the iodine signal, further improving the diagnostic quality in large numbers of patients. Smaller collimation of the UHR mode also increases the probability of motion artifacts. In addition, some vascular kernels, especially lower-level Bv kernels, have edge correction algorithms that result in artificial-looking images. This can usually be mitigated using sharper kernels (Fig. 12C, D).

A practical challenge of PCCT is the large amount of data generated owing to thinner slices and multiple image types. This can increase the transfer time from the scanner to the PACS, delaying final reporting. In addition, additional storage space must be provided for the excess data, which has financial implications. To mitigate data overload, efforts should be made to select and optimize only the images

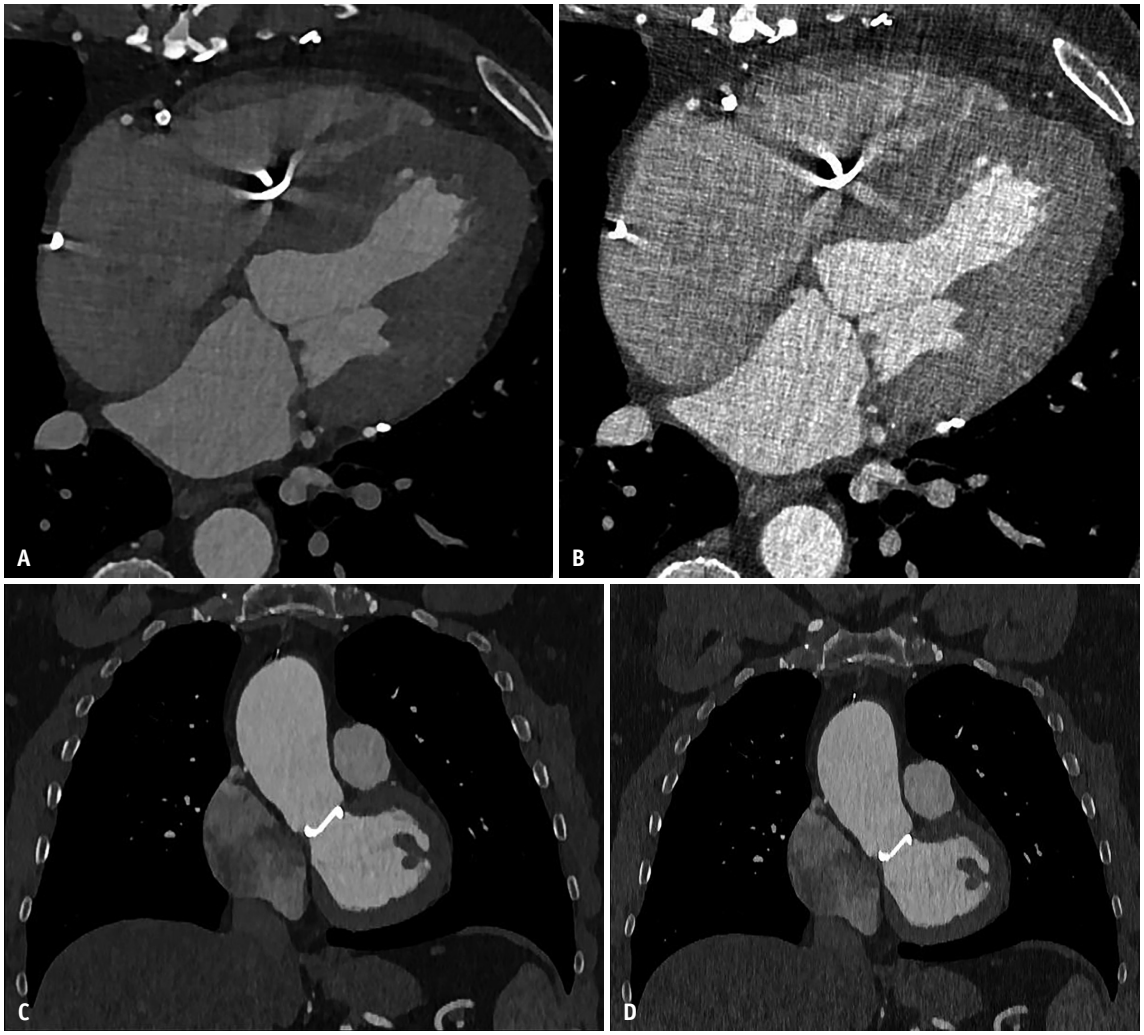

Fig. 12. Challenges of PCCT. **A:** Axial coronary CTA from PCCT in a 61-year-old male using Bv48 filter shows good image quality. **B:** Axial coronary CTA in the same patient using sharper Bv60 filter shows increased noise. Noise is a key limitation of ultra-high-resolution images, especially with thin slices, sharp kernels, and high matrix size. **C:** Coronal CTA from PCCT in a 45-year-old male using Bv44 filter shows artificially "painted" margins. **D:** Coronal CTA in the same patient using sharper Bv56 filter shows improved, more natural image appearance. PCCT = photon-counting CT, CTA = CT angiography

https://doi.org/10.3348/kjr.2024.0261

Korean Journal of Radiology
KJR

necessary for interpretation.

CONCLUSION

PCCT is an innovative CT technology that offers several advantages for cardiovascular imaging. UHR capabilities enhance the visualization of small vessels, heavily calcified vessels, and stents, thereby improving the accuracy of cardiovascular CT. The improved quality of multienergy images provides enhanced iodine signal, reduced artifacts, improved lesion characterization, calcium or iodine separation, and radiation dose reduction. PCCT also provides lower image noise and higher iodine CNR. Optimal use of PCCT requires an understanding of the various technical parameters that can be adjusted for specific clinical applications.

Conflicts of Interest

The authors have no potential conflicts of interest to disclose.

Author Contributions

Conceptualization: Prabhakar Shantha Rajiah, Phillip M. Young. Methodology: Prabhakar Shantha Rajiah, Shuai Leng, Phillip M. Young. Supervision: Prabhakar Shantha Rajiah, Phillip M. Young, Shuai Leng. Validation: all authors. Visualization: all authors. Writing—original draft: Prabhakar Shantha Rajiah, James M. Williams, Michael LaVere. Writing—review & editing: all authors

ORCID IDs

Prabhakar Shantha Rajiah
https://orcid.org/0000-0001-7538-385X
James M. Williams
https://orcid.org/0000-0002-9936-9275
Michael LaVere
https://orcid.org/0009-0007-0618-2860
Shuai Leng
https://orcid.org/0000-0002-6453-9481

Funding Statement

None

REFERENCES

1. Rajendran K, Petersilka M, Henning A, Shanblatt ER, Schmidt B, Flohr TG, et al. First clinical photon-counting detector CT system: technical evaluation. *Radiology* 2022;303:130-138
2. Imaging Technology News. Siemens Healthineers expands photon-counting CT portfolio [accessed on September 2, 2025]. Available at: https://www.itnonline.com/content/siemens-healthineers-expands-photon-counting-ct-portfolio
3. Rajendran K, Canan A, Rajiah PS. Cardiac imaging using photon counting CT - benefits, challenges and prospects. *Int J Cardiovasc Imaging* 2025 Aug 30 [Epub]. http://doi.org/10.1007/s10554-025-03491-x
4. Kalisz K, Halliburton S, Abbara S, Leipsic JA, Albrecht MH, Schoepf UJ, et al. Update on cardiovascular applications of multienergy CT. *Radiographics* 2017;37:1955-1974
5. Esquivel A, Ferrero A, Mileto A, Baffour F, Horst K, Rajiah PS, et al. Photon-counting detector CT: key points radiologists should know. *Korean J Radiol* 2022;23:854-865
6. Nehra AK, Rajendran K, Baffour FI, Mileto A, Rajiah PS, Horst KK, et al. Seeing more with less: clinical benefits of photon-counting detector CT. *Radiographics* 2023;43:e220158
7. Writing Committee Members; Gulati M, Levy PD, Mukherjee D, Amsterdam E, Bhatt DL, Birtcher KK, et al. 2021 AHA/ACC/ASE/CHEST/SAEM/SCCT/SCMR guideline for the evaluation and diagnosis of chest pain: a report of the American College of Cardiology/American Heart Association Joint Committee on clinical practice guidelines. *J Am Coll Cardiol* 2021;78:e187-e285
8. Kwan AC, Gransar H, Tzolos E, Chen B, Otaki Y, Klein E, et al. The accuracy of coronary CT angiography in patients with coronary calcium score above 1000 Agatston units: comparison with quantitative coronary angiography. *J Cardiovasc Comput Tomogr* 2021;15:412-418
9. Hagar MT, Soschynski M, Saffar R, Rau A, Taron J, Weiss J, et al. Accuracy of ultrahigh-resolution photon-counting CT for detecting coronary artery disease in a high-risk population. *Radiology* 2023;307:e223305
10. Kotronias RA, de Maria GL, Xie C, Thomas S, Chan K, Portolan L, et al. Benchmarking photon-counting computed tomography angiography against invasive assessment of coronary stenosis: implications for severely calcified coronaries. *JACC Cardiovasc Imaging* 2025;18:572-585
11. Halfmann MC, Bockius S, Emrich T, Hell M, Schoepf UJ, Laux GS, et al. Ultrahigh-spatial-resolution photon-counting detector CT angiography of coronary artery disease for stenosis assessment. *Radiology* 2024;310:e231956
12. Vecsey-Nagy M, Tremamunno G, Schoepf UJ, Gnasso C, Zsarnóczay E, Fink N, et al. Intraindividual comparison of ultrahigh-spatial-resolution photon-counting detector CT and energy-integrating detector CT for coronary stenosis measurement. *Circ Cardiovasc Imaging* 2024;17:e017112
13. Sharma SP, Verhemel S, Hirsch A, van der Bie J, Dijkshoorn ML, Daemen J, et al. Diagnostic performance of high and ultra-high-resolution photon counting CT for detection of coronary artery disease in patients evaluated for transcatheter aortic valve implantation. *Int J Cardiovasc Imaging* 2024 Nov 4 [Epub]. http://doi.org/10.1007/s10554-024-03273-x
14. Sakai K, Shin D, Singh M, Malik S, Dakroub A, Sami Z, et al.

Diagnostic performance and clinical impact of photon-counting detector computed tomography in coronary artery disease. *J Am Coll Cardiol* 2025;85:339-348
15. Vecsey-Nagy M, Emrich T, Tremamunno G, Kravchenko D, Taha Hagar M, Laux GS, et al. Cost-effectiveness of ultrahigh-resolution photon-counting detector coronary CT angiography for the evaluation of stable chest pain. *J Cardiovasc Comput Tomogr* 2025;19:106-112
16. Yalon M, Inoue A, Thorne JE, Lee YS, Johnson MP, Esquivel A, et al. Infrapopliteal segments on lower extremity CTA: prospective intraindividual comparison of energy-integrating detector CT and photon-counting detector CT. *AJR Am J Roentgenol* 2024;222:e2329778
17. Ghibes P, Hagen F, Weissinger M, Wrazidlo R, Nikolaou K, Levitin A, et al. Diagnostic performance of photon-counting CT angiography in peripheral artery disease compared to DSA as gold standard. *Eur J Radiol* 2025;182:111834
18. McCollough CH, Winfree TN, Melka EF, Rajendran K, Carter RE, Leng S. Photon-counting detector computed tomography versus energy-integrating detector computed tomography for coronary artery calcium quantitation. *J Comput Assist Tomogr* 2024;48:212-216
19. Wolf EV, Halfmann MC, Schoepf UJ, Zsarnoczay E, Fink N, Griffith JP 3rd, et al. Intra-individual comparison of coronary calcium scoring between photon counting detector- and energy integrating detector-CT: effects on risk reclassification. *Front Cardiovasc Med* 2023;9:1053398
20. Kalisz K, Buethe J, Saboo SS, Abbara S, Halliburton S, Rajiah P. Artifacts at cardiac CT: physics and solutions. *Radiographics* 2016;36:2064-2083
21. Allmendinger T, Nowak T, Flohr T, Klotz E, Hagenauer J, Alkadhi H, et al. Photon-counting detector CT-based vascular calcium removal algorithm: assessment using a cardiac motion phantom. *Invest Radiol* 2022;57:399-405
22. Mergen V, Rusek S, Civaia F, Rossi P, Rajagopal R, Bättig E, et al. Virtual calcium removal in calcified coronary arteries with photon-counting detector CT-first in-vivo experience. *Front Cardiovasc Med* 2024;11:1367463
23. Narula J, Chandrashekhar Y, Ahmadi A, Abbara S, Berman DS, Blankstein R, et al. SCCT 2021 expert consensus document on coronary computed tomographic angiography: a report of the society of cardiovascular computed tomography. *J Cardiovasc Comput Tomogr* 2021;15:192-217
24. van der Bie J, Sharma SP, Hirsch A, Boccalini S, van Mieghem NM, Dijkshoorn ML, et al. Coronary stent imaging with photon-counting detector CT. *Radiol Cardiothorac Imaging* 2025;7:e240338
25. Adolf R, Ried I, Will A, Hendrich E, Bressem K, Engel LC, et al. Assessing beam hardening artifacts in coronary stent imaging using different CT acquisition parameters on photon-counting detector computed tomography. *Int J Cardiovasc Imaging* 2025 Apr 10 [Epub]. http://doi.org/10.1007/s10554-025-03392-z
26. Hagar MT, Soschynski M, Saffar R, Molina-Fuentes MF, Weiss J, Rau A, et al. Ultra-high-resolution photon-counting detector CT in evaluating coronary stent patency: a comparison to invasive coronary angiography. *Eur Radiol* 2024;34:4273-4283
27. Qin L, Zhou S, Dong H, Li J, Zhang R, Yang C, et al. Improvement of coronary stent visualization using ultra-high-resolution photon-counting detector CT. *Eur Radiol* 2024;34:6568-6577
28. Stein T, von Zur Muhlen C, Verloh N, Schürmann T, Krauss T, Soschynski M, et al. Evaluating small coronary stents with dual-source photon-counting computed tomography: effect of different scan modes on image quality and performance in a phantom. *Diagn Interv Radiol* 2025;31:29-38
29. Dogra S, Madhavan A, Moonis G. Neuroimaging applications of photon-counting CT. *J Comput Assist Tomogr* 2026;50:46-53
30. Lan Y, Liu R, Guo L, Zhang C, Zhang H, Huang J, et al. Advancing preoperative planning in perforator flap surgery with photon-counting computed tomography angiography: less challenges with more precision. *Aesthetic Plast Surg* 2025;49:4888-4900
31. Yousif P, Linch F, Rajiah P, Collins JD, Favazza CP, Ferrero A, et al. Photon counting detector CTA for prostate artery embolization pre-procedure planning and intra-procedural guidance. *CVIR Endovasc* 2025;8:55
32. Rajiah PS, Dunning CAS, Rajendran K, Tandon YK, Ahmed Z, Larson NB, et al. High-pitch multienergy coronary CT angiography in dual-source photon-counting detector CT scanner at low iodinated contrast dose. *Invest Radiol* 2023;58:681-690
33. Higaki F, Morimitsu Y, Iguchi T, Saito H, Takaki H, Nakagoshi A, et al. Photon-counting detector CT: potential for 75% reduction in contrast medium amount: a phantom study. *Acta Med Okayama* 2024;78:135-142
34. Hennes JL, Huflage H, Grunz JP, Hartung V, Augustin AM, Patzer TS, et al. An intra-individual comparison of low-keV photon-counting CT versus energy-integrating-detector CT angiography of the aorta. *Diagnostics (Basel)* 2023;13:3645
35. Cury RC, Leipsic J, Abbara S, Achenbach S, Berman D, Bittencourt M, et al. CAD-RADS™ 2.0–2022 coronary artery disease-reporting and data system. *J Cardiovasc Comput Tomogr* 2022;16:536-557
36. Mergen V, Eberhard M, Manka R, Euler A, Alkadhi H. First in-human quantitative plaque characterization with ultra-high resolution coronary photon-counting CT angiography. *Front Cardiovasc Med* 2022;9:981012
37. Vecsey-Nagy M, Tremamunno G, Schoepf UJ, Gnasso C, Zsarnóczay E, Fink N, et al. Coronary plaque quantification with ultrahigh-spatial-resolution photon-counting detector CT: intraindividual comparison with energy-integrating detector CT. *Radiology* 2025;314:e241479
38. Skoog S, Good E, Henriksson L, Sandstedt M, Persson A, Tesselaar E. Effect of reconstruction kernel and virtual monoenergetic imaging on segmentation-based measurement of coronary plaque volume with photon-counting CT. *Invest Radiol* 2025;60:602-608
39. Sartoretti T, Mergen V, Dzaferi A, Allmendinger T, Manka R, Alkadhi H, et al. Effect of temporal resolution on calcium

scoring: insights from photon-counting detector CT. *Int J Cardiovasc Imaging* 2025;41:615-625
40. Eberhard M, Mergen V, Higashigaito K, Allmendinger T, Manka R, Flohr T, et al. Coronary calcium scoring with first generation dual-source photon-counting CT-first evidence from phantom and in-vivo scans. *Diagnostics (Basel)* 2021;11:1708
41. Hur J, Kim YJ, Lee HJ, Nam JE, Hong YJ, Kim HY, et al. Cardioembolic stroke: dual-energy cardiac CT for differentiation of left atrial appendage thrombus and circulatory stasis. *Radiology* 2012;263:688-695
42. Haag NP, Michael AE, Lennartz S, Panknin C, Niehoff JH, Borggrefe J, et al. Coronary artery calcium scoring using virtual versus true noncontrast images from photon-counting coronary CT angiography. *Radiology* 2024;310:e230545
43. Emrich T, Aquino G, Schoepf UJ, Braun FM, Risch F, Bette SJ, et al. Coronary computed tomography angiography-based calcium scoring: in vitro and in vivo validation of a novel virtual noniodine reconstruction algorithm on a clinical, first-generation dual-source photon counting-detector system. *Invest Radiol* 2022;57:536-543
44. Mergen V, Ghouse S, Sartoretti T, Manka R, Euler A, Kasel AM, et al. Cardiac virtual noncontrast images for calcium quantification with photon-counting detector CT. *Radiol Cardiothorac Imaging* 2023;5:e220307
45. Sharma SP, van der Bie J, van Straten M, Hirsch A, Bos D, Dijkshoorn ML, et al. Coronary calcium scoring on virtual non-contrast and virtual non-iodine reconstructions compared to true non-contrast images using photon-counting computed tomography. *Eur Radiol* 2024;34:3699-3707
46. Fink N, Emrich T, Schoepf UJ, Zsarnoczay E, O'Doherty J, Halfmann MC, et al. Improved detection of small and low-density plaques in virtual noncontrast imaging-based calcium scoring at photon-counting detector CT. *Radiol Cardiothorac Imaging* 2024;6:e230328
47. Ko SM, Choi JW, Song MG, Shin JK, Chee HK, Chung HW, et al. Myocardial perfusion imaging using adenosine-induced stress dual-energy computed tomography of the heart: comparison with cardiac magnetic resonance imaging and conventional coronary angiography. *Eur Radiol* 2011;21:26-35
48. Wang R, Yu W, Wang Y, He Y, Yang L, Bi T, et al. Incremental value of dual-energy CT to coronary CT angiography for the detection of significant coronary stenosis: comparison with quantitative coronary angiography and single photon emission computed tomography. *Int J Cardiovasc Imaging* 2011;27:647-656
49. Pontana F, Gkizas C, Rodriguez Musso A, Longere B. Initial insights into CT myocardial perfusion imaging using photon-counting detector technology. *J Cardiovasc Comput Tomogr* 2025;19(Supplement):S25-S26
50. Tremamunno G, Varga-Szemes A, Kravchenko D, Laghi A, Bamberg F, Halfmann MC, et al. Accuracy of photon-counting detector CT-based iodine maps for myocardial late enhancement detection. *Eur Radiol* 2025;35:7074-7083
51. Symons R, Krauss B, Sahbaee P, Cork TE, Lakshmanan MN, Bluemke DA, et al. Photon-counting CT for simultaneous imaging of multiple contrast agents in the abdomen: an in vivo study. *Med Phys* 2017;44:5120-5127
52. Treibel TA, Fontana M, Steeden JA, Nasis A, Yeung J, White SK, et al. Automatic quantification of the myocardial extracellular volume by cardiac computed tomography: synthetic ECV by CCT. *J Cardiovasc Comput Tomogr* 2017;11:221-226
53. Mergen V, Sartoretti T, Klotz E, Schmidt B, Jungblut L, Higashigaito K, et al. Extracellular volume quantification with cardiac late enhancement scanning using dual-source photon-counting detector CT. *Invest Radiol* 2022;57:406-411
54. Gkizas C, Longere B, Sliwicka O, Musso AR, Lemesle G, Croisille C, et al. Photon-counting CT-derived extracellular volume in acute myocarditis: comparison with cardiac MRI. *Diagn Interv Imaging* 2025;106:255-263
55. Aquino GJ, O'Doherty J, Schoepf UJ, Ellison B, Byrne J, Fink N, et al. Myocardial characterization with extracellular volume mapping with a first-generation photon-counting detector CT with MRI reference. *Radiology* 2023;307:e222030
56. Gnasso C, Pinos D, Schoepf UJ, Vecsey-Nagy M, Aquino GJ, Fink N, et al. Impact of reconstruction parameters on the accuracy of myocardial extracellular volume quantification on a first-generation, photon-counting detector CT. *Eur Radiol Exp* 2024;8:70
57. Turrion Gomollon AM, Mergen V, Sartoretti T, Polacin M, Nakhostin D, Puippe G, et al. Photon-counting detector CT angiography for endoleak detection after endovascular aortic repair: triphasic CT with true noncontrast versus biphasic CT with virtual noniodine imaging. *Invest Radiol* 2023;58:816-821
58. Si-Mohamed SA, Sigovan M, Hsu JC, Tatard-Leitman V, Chalabreysse L, Naha PC, et al. In vivo molecular K-edge imaging of atherosclerotic plaque using photon-counting CT. *Radiology* 2021;300:98-107
59. Mihailovic JM, Bruesewitz MR, Swicklik JR, Yalon M, Rajiah PS, Fletcher JG, et al. Simultaneous high-pitch multi-energy CT pulmonary angiography using a dual-source photon-counting-detector CT: a phantom experiment. *J Appl Clin Med Phys* 2024;25:e14496
60. Yalon M, Hoodeshenas S, Chan A, Horst KK, Crum I, Thorne JE, et al. Improved pulmonary artery evaluation using high-pitch photon-counting CT compared to high-pitch conventional or routine-pitch conventional dual-energy CT. *J Comput Assist Tomogr* 2024;48:897-905

 https://doi.org/10.3348/kjr.2024.0261